Spring 2023

Experimental Observation of Sphere Symmetric Isolated Single Droplet Combustion in a Converging Channel

Mason Carrington Williams

EXPERIMENTAL OBSERVATION OF SPHERE SYMMETRIC ISOLATED SINGLE DROPLET COMBUSTION IN A CONVERGING CHANNEL

by

Mason Carrington Williams

Bachelor of Science in Engineering
University of South Carolina, 2022

Submitted in Partial Fulfillment of the Requirements

For the Degree of Master of Science in

Mechanical Engineering

College of Engineering and Computing

University of South Carolina

2023

Accepted by:

Sang Hee Won, Director of Thesis

Tanvir Farouk, Reader

Cheryl L. Addy, Interim Vice Provost and Dean of the Graduate School

DEDICATION

I would like to dedicate this work to my grandfather David Reid Williams Jr. or as I knew him, Papa D. He heard me complain about or be excited about how this work was going more than anyone else. He was my biggest fan. Sadly, he passed away just before I completed this thesis work.

ACKNOWLEDGEMENTS

I would like to thank my advisor Dr. Sang Hee Won along with all the members of our lab. Especially Claire Dixon, who worked alongside me through this project.

ABSTRACT

Spherically symmetric isolated single droplet combustion has been observed mainly in microgravity conditions. This study sought to determine if spherically symmetric combustion can be produced in a lab-scale experiment using flow acceleration to counteract the effects of buoyancy. The experiment was conducted in a converging channel that decreased in width along its length to accelerate the flow and limit the formation of a boundary layer. The rate at which the area decreased was governed by the initial velocity condition set at the channel inlet.

The droplets were generated using a piezoelectric actuator which forced fuel out of an injector with a very narrow inner diameter. A thin metal disk at the top of the main fuel reservoir allowed the piezoelectric to directly influence the pressure of the fluid in the system. The flowrate of fuel through the system was held constant by a syringe pump. The diameter of droplets produced was approximately 0.5 – 0.6 mm and the fuels used were n-Heptane and ethanol.

It was found that the initial velocity at the inlet of the converging channel was 1 m/s. This velocity was used to define the curvature needed to observe sphere symmetric flames. A transition from laminar flow to turbulent flow within the converging channel due to the boundary layer growth was found. The droplet diameter and flame diameter were observed at various points along the length of the channel. The droplet diameter was determined using backlight imaging and a Photron Fastcam SA-Z highspeed camera. To observe the flame diameter, an Andor iStar intensified complementary metal oxide semiconductor (ICMOS) camera was used.

From this study, it was concluded that spherically symmetric flames can be created and observed under normal gravitational conditions utilizing accelerated fluid flow through a converging channel. The nature of this apparatus allows for further investigation into spherically symmetric isolated droplet combustion utilizing laser diagnostic techniques and nuclear magnetic resonance (NMR) imaging to analyze the composition of partially combusted samples. This will allow further study into the effects of preferential vaporization on multi-component mixtures.

TABLE OF CONTENTS

LIST OF FIGURES

LIST OF SYMBOLS

Q	Volumetric flow rate
f	Flowrate
t	Time
v_0	Initial velocity, which is equal to the velocity at time t = 0
v	Velocity at a given time t
a	Linear acceleration
Δx	Change in position
d	Diameter

LIST OF ABBREVIATIONS

ICMOS ..... Intensified Complementary Metal Oxide Semiconductor

ISS ..... International Space Station

JAMIC ..... Japan Microgravity Center

NASA ..... National Aeronautics and Space Administration

NMLC ..... National Microgravity Laboratory

NMR ..... Nuclear Magnetic Resonance

CHAPTER 1

INTRODUCTION

Investigations into droplet combustion began over 80 years ago in the late 1940s. Godsave is one of the pioneers of droplet combustion, detailing an experiment conducted at the National Gas Turbine Establishment of the United Kingdom to determine the factors which influence the rate of burning of droplets in a fuel spray [1]. Many early experiments studied droplets by suspending them on thin silica filaments or other thin supporting fibers. The results presented by Godsave follow an early understanding of the d-squared law of droplet combustion. Initially termed the first power of the diameter law, Godsave's concept relates the droplet diameter and time to determine the burning rate [2]. Further theoretical analysis of Godsave's work was conducted by Goldsmith and Penner. To more fully develop a theoretical understanding of single droplet combustion, several assumptions were made including but not limited to: spherical droplets, uniform temperature and pressure, spherical flame, convective effects can be ignored, and steady state conditions for fixed droplet sizes [3]. The d-squared law was introduced by Kumagai and Isoda in a letter within a journal regarding the combustion of fuel droplets in response to Godsave's work [4]. Kumagai and Isoda's work was expanded upon in a publication in 1957 which noted the differences imposed by natural convection on the burning of a droplet compared to the spherically symmetric model used for theoretical calculations. To address the issue of natural convection, the

experiments were conducted in a chamber that fell freely with constant gravitational acceleration [5]. Kumagai continued to investigate single droplet combustion and was able to more closely model spherically symmetric conditions by developing an experimental assembly which did not involve suspending the droplet on a filament [6]. In conjunction with Okajima, Kumagai continued investigating droplet combustion within a freely falling chamber. The initial experiments had a short observation time for the burning process, so subsequent investigations doubled the experimental time to reach 1 second. This extended experiment also explored the effects of weak forced convection by allowing the combusting droplet to move relative to the falling chamber [7].

As notably explored by Kumagai, gravity and natural convection affect the manner in which freely falling fuel droplets burn. To create a spherically symmetric droplet throughout the entire combustion process, the gravitational effect of buoyancy must be negated by an opposing force. The most common example illustrating buoyancy impacting the shape of a flame is a candle flame. A candle flame is round at the bottom and pointed and elongated at the top. This difference in shape is due to the gaseous elements of fuel and air rising due to buoyancy when heated, drawing the flame upwards. In an ideal setting without buoyancy, the flame would be spherical. The initial manner of creating an environment free from buoyancy involved using a freely falling chamber, as first seen with Kumagai in the 1950s [5]. However, this chamber did not implement free droplet combustion and relied on a supporting filament, so a second generation design was developed by Kumagai in the 1970s [6]. Other experimentation with freely falling chambers and free droplets was conducted in the same decade by various investigators. Knight and Williams used a freely falling chamber which could provide 2.2 seconds of

residence time to offset the effects of buoyancy in their research. While Kumagai's experiments were conducted in a surrounding gas environment that was composed of air, Knight and Williams used a surrounding gas environment of a mixture of oxygen and nitrogen in their freely falling chamber. Knight and Williams used Kumagai's work as a starting point for their own experiment, but increased the residence time, thus allowing for investigating if quasi-steady state burning could be achieved in the gas phase [8].

Buoyancy is the central problem with conducting experiments in normal gravity conditions. The density differences brought on by the drastic changes in temperature that occur during combustion processes invariably generate buoyant effects in the presence of gravity. The effects of buoyancy do not allow for the assumptions that drastically simplify the calculations and make numerical modelling possible to be made, so buoyancy must be negated for an idealized experimental setup [9]. Examples of such setups have been constructed on Earth, in addition to conducting experiments in true microgravity environments, such as on the International Space Station (ISS). The simplest of the developed facilities to study droplet combustion in microgravity are known as drop towers. Drop towers are the most accessible of the microgravity facilities and have been developed on a small scale by individual researchers with testing times less than 1 second. In addition, larger drop towers which require over 5 meters of available distance have been constructed. The small scale drop towers involve freely falling chambers and may be improved upon with the use of drag shields, for which an inner test chamber falls within a larger freely falling chamber so that the drag effects of extended free fall, for fall times exceeding 0.5 seconds, may be minimized [9].

The more complex drop towers can reach up to 10 seconds of observable experimentation time. The NASA Glen Research Center is home to two of these sophisticated drop towers. The facility includes a drop tower capable of 2.2 seconds of observation time with a free fall height of 27 meters, as well as a another drop tower capable of 5.2 seconds of observation with a free fall height of 143 meters. The freely falling experimental apparatus experiences only one force, residual air drag. The result is that the system experiences exceptionally low gravitational acceleration equivalent to an order of 10^{-5} g maximum. The two drop towers have different recovery systems that promote deceleration. The shorter of the two utilizes a sand pit which is penetrated by deceleration spikes attached to the exterior of the experimental apparatus. The longer uses polystyrene pellets to fill the space between the experimental apparatus and a deceleration container [10]. Regardless of the method of deceleration, drop tower free fall facilities with extended experimental observation times face a considerable shock load at the termination of the fall. This impact has limited the ability to adapt common optical diagnostic methods for experiments conducted in the extended drop towers due to the equipment being unable to sustain such forces without suffering significant damage [9]. Another limitation of ground-based experiments is that large droplets cannot be sufficiently observed due to the short windows of experimentation available [11].

Despite the increase of observable experimental time offered in these free fall facilities compared to the small scale drop towers, the experimental time is still capped at 10 seconds in the tallest of these facilities. In order to increase the time of study for combustion experiments, especially to evaluate if steady-state conditions have been able to be reached, other methods of inducing microgravity have been explored. One of these

methods is to use aircraft in parabolic flight. However, aircraft typically are unable to exactly execute precise maneuvers to create free fall trajectories resulting in reduced gravity with low, but non-negligible, buoyancy effects. The observation time is between 15 and 20 seconds with several of these windows of observation occurring in one flight period. The most significant impact of aircraft-based experiments the development and implementation of techniques to be used in space-based experiments [9].

Space-based experiments regarding combustion were conducted during the time that the Skylab satellite was operational from 1973-1974. In 1992, combustion experiments were conducted on the Space Shuttle to examine candle flames [9]. Later in the 1990s, microgravity experimentation was conducted in space using Spacelab on a space shuttle flight. The droplets investigated during this Spacelab experiment ranged from 2 to 5 mm in diameter and contained both single element droplets of methanol as well as binary mixtures of methanol and water, methanol and dodecanol, and heptane and hexadecane. The experiment validated theoretical predictions of extinction diameter increasing with initial droplet diameter in addition to using forced convective flow to increase the burning rate [12]. This experiment benefitted from being conducted in space due to the limitation of gathering full combustion histories for the size of droplets considered using ground-based facilities.

The construction of the ISS saw new opportunities for microgravity combustion experimentation because of the increased duration for which experiments could be conducted. Another benefit to the new space station was the ability to conduct experiments in a variety of ambient pressure conditions and compositions of surrounding atmosphere. Initial isolated droplet experimentation on the ISS investigated radiative and

diffusive extinction using heptane and methanol as well as determined the concentration level of oxygen under which quasi-steady combustion is not supported, known as the limiting oxygen index, to ensure fire safety on the spacecraft [13]. The extended investigative ability supported by conducting such combustion experiments on the ISS has allowed for the collection of measurements which may be used to help further develop several numerical and computational models as well as a theoretical understanding of droplet combustion. A unique phenomenon able to be investigated on the ISS utilizing isolated single droplet combustion experimentation is cool flames. This second stage of combustion was noticed during experiments conducted with n-heptane intended to investigate radiative extinction behavior at atmospheric pressure in a surrounding environment of nitrogen and oxygen. In this experiment, the end of the high temperature droplet burning transitioned to behavior of low temperature, constant burning rate. In this stage, there was no visible flame but quasi-steady vaporization occurred and led to extinction by diffusion at a finite droplet size [14]. The observation of this behavior led to differences with classical assumptions regarding premixed cool flames due to the second stage of combustion being initiated from hot ignition that then transitions to lower temperatures via heat loss. Such an effect has not yet been seen in ground-based single isolated droplet combustion studies. In general, the radiative extinction aspect of droplet combustion is most easily investigated during space-based experiments. One limitation of space-based experiments is that droplets of initial diameter less than 1 mm are not easily studied. This is due to the relative lack of gravity; when the droplet diameter becomes too small, its trajectory becomes erratic.

In addition to the increased ability to investigate spherically symmetric droplet combustion during space-based experiments or other negligible gravity conditions, there have also been recent increases in the computational ability to numerically model and evaluate droplet combustion phenomena. Some of these models have been developed to reproduce the results of experiments [15] while others recognized how some experimental effects were not present in the model, such as convective effects and sooting [16]. The relevant developed models are transient, sphere symmetric, and involve detailed chemical kinetics that govern the gas phase portion of the combustion reaction [15-18].

Over time, more detailed models have been able to be developed, using previously developed models and their comparison to experimental data as a baseline [15]. For example, Kazakov et al. included gas-phase radiative heat transfer and water condensation on the droplet surface in their model. Such elements had never previously ~~not~~ been considered in prior models for ethanol [7, 19]. Despite the models becoming more detailed, the full range of chemical processes occurring during the combustion process are not described because of the large number of species and reactions involved. Marchese et al. used a compact model with 51 species and 282 reactions to describe the gas phase of their n-heptane and n-hexadecane model as an example to provide a sense of scale for the expansive size of even the "compact" models [16]. The more modern modeling performed by Liu et al. included admittance that previous assumptions held in the classical theory of droplet burning have been proven to be false such as the quasi-steady behavior of the gas phase, constant temperature and pressure, negligible radiation,

no soot formation, and a single step reaction at the flame [17]. However, the classical theory can be used as a starting point for numerical analyses.

Despite the merits and contributions made to droplet combustion studies from space-based experiments, there is still a need to conduct experiments on Earth. Droplets of small diameter, that is less than 1 mm, are only able to be used in ground-based experiments. Beyond the drop towers developed at NASA's Glenn Research Center, other drop towers have been developed in the subsequent years to increase the accessibility of these facilities as well as provide a range of fall distances and times of observation. One such example is found in China at the National Microgravity Laboratory (NMLC), built in the mid-1990s. The NMLC drop tower is 116 m tall with an experimental time of 3.5 seconds. Other ground-based drop towers are found in Japan at the Japan Microgravity Center (JAMIC), where the largest drop tower in the world is located that has a residence time of 10 seconds. Another drop tower at JAMIC has an residence time of 4.5 seconds. One key improvement of the JAMIC drop towers compared to the NASA drop towers is the reduced shock load experienced by the experimental apparatus during the deceleration process. Another drop tower facility is located in Germany with a residence time of 4.7 seconds. In addition to the previously listed large scale drop tower facilities, smaller facilities have been developed at universities with observation times of less than 1 second [20]. These smaller facilities provide a means of obtaining some experimental data that could also be found in the larger scale facilities without the higher associated cost of those facilities.

One suggested alternative to drop towers is known as a drop tube. Wang et al. developed the drop tube as a type of flow tube which would support the idealizations

made in the classical assumptions of droplet combustion as spherically symmetric in an infinite environment. The infinite environment assumption requires negligible convective effects either through force or buoyancy. To support the minimization of convective effects, a contour was suggested for the walls of the flow tube rather than utilizing the more traditional design of constant cross-sectional area. The walls of the flow tube will experience the growth of a boundary layer, but the central core of the flow may be approximated as one dimensional and inviscid [21]. Advantages to this experimental design include the ability to use a variety of instrumentation to observe and measure phenomena that are not available for use in drop tower experiments, as well as the ability to examine smaller droplet sizes.

Similar in design to the drop tube and most influential to this study, Choi proposed a ground-based reduced gravity experiment that utilized accelerating flow to match the droplet velocity along the axial direction. Accelerating the flow would make the relative motion in comparison to the droplet negligible. Choi's design for the geometry of the tube was based on a rectangular cross-section with a constant width; this design served as the basis for the design of the converging channel used in this study. The flat surfaces composing the front and back of the tube were transparent to facilitate use of optical instruments. A tube with curved walls corresponding to a circular cross section was also considered, but the distortion that would result from the curved surfaces for optical measurements rendered the rectangular cross-sectioned tube more favorable. Other inspiration for the experimental approach used in this study from Choi is the use of hot-wire ignition [22].

Overall, the purpose of this study is to determine a method for supporting sphere symmetric droplet combustion outside of a traditional reduced gravity environment. The ability to do so will allow for investigations that would not be possible in drop towers or space-based experiments, which include investigating the extent of preferential vaporization in multi-component fuels.

CHAPTER 2

EXPERIMENTAL SETUP

The experimental setup consists of several parts, each of which underwent an optimization process either in regard to either its design or its operation. The setup is composed of the following parts: the injector, the droplet generator, the heating coil, the converging channel, the general structure, and the air pump. The most complex portion of the setup is the injector and droplet generator. The injector has a very small exit diameter to capitalize on the pressure wave created by the piezoelectric actuator of the droplet generator. The initial failed method of fabrication for the injector utilized a glass capillary tube attached to the end of a small piece of metal tubing with a narrow inner diameter. The capillary tube was heated and stretched to decrease its exit diameter to create a small exit diameter. While this method of fabrication provided an exceptionally small exit diameter, the brittle nature of the capillary tube coupled with the inconsistency of the manufacturing process meant that a different method of fabrication would be more successful. The new method of fabrication was to barely insert a small metal capillary tube into the piece of metal tubing, then use epoxy to fix the capillary tube inside the tubing. The metal capillary tube was then sanded down so that it protruded minimally from the end of the larger metal tube. This final design for the injector worked due to the drastic and sudden decrease of cross-sectional area at the exit, concentrating the pressure

wave from the droplet generator and maximizing the ability to consistently create droplets.

The droplet generator consists of a two-part system made up of a piezoelectric actuator and a syringe pump, as seen in Figs. [2.1 and 2.2]. The piezoelectric actuator presses a thin metal disc fixed to the top of a small conical reservoir full of the liquid fuel to be pushed down into the injector. The fuel is fed into plastic tubing leading to the reservoir from a syringe by a syringe pump (New Era Pump Systems, Inc. Model 1000) operating at a set flow rate. The optimal flowrate was determined to be 1.8 mL/hr by trial and error. A Siglent SDG 2042X function generator creates the waveforms that control the piezoelectric actuator. The waveforms are boosted by a Thor Labs HVA200 high voltage amplifier before going to the piezoelectric actuator. The pulse waveform was selected after a process of trial and observation with the other available waveform options, such as sinusoidal, ramp, and square. Beyond just the shape of the waveform, other variables are controlled by the function generator. The features that were found to be most important for the generation of droplets are the pulse width, frequency, rise and fall edge, voltage, and delay. The pulse width governed how long the piezoelectric actuator remained depressed. Increasing the pulse width allowed for droplets to be created at lower voltages which was essential in avoiding creating droplet sprays rather than single isolated droplets. The frequency of the pulses governed how often the droplets were created. Changing the frequency necessitated changing the other governing parameters of the waveform to retain ideal conditions for droplet production. The frequency is also bound to the flowrate of the liquid fuel set on the syringe pump as seen

in the theoretical determination of droplet diameter. The flowrate of fuel is volumetric and is represented as volume over time in the following equation,

$$Q = {}^{V}/_{t} \tag{2.1}$$

The definition of frequency as the inverse of time allows the equation for volumetric flowrate to be rewritten as follows,

$$Q = f \cdot V \tag{2.2}$$

Due to the assumption of the droplet being spherical, the volume of the droplet as a function of the diameter is defined as follows,

$$V = \frac{\pi}{6} d^3 \tag{2.3}$$

Utilizing this definition in the equation for the volumetric flowrate,

$$Q = f \cdot \frac{\pi}{6} d^3 \tag{2.4}$$

Rearranging equation (3.4) for the diameter yields the theoretical droplet diameter as a function of the volumetric flowrate of the fuel and frequency of the droplet generation,

$$d = \sqrt[3]{\frac{6Q}{\pi f}} \tag{2.5}$$

As flowrate increases, the voltage required to eject liquid fuel is reduced due to increased internal pressure. The rise edge governs how long it takes to reach the maximum voltage output from zero. The fall edge governs how long it takes to reach zero after achieving the maximum voltage output. The rise edge and fall edge have a less observable effect on droplet creation but are important in ensuring consistency in the droplets generated. The

rise edge is greater than the fall edge by a factor of ten and aids in maintaining the generation of isolated single droplets rather than multiple droplets. A short fall edge is utilized to prevent the droplet leaving the end of the injector with a negative initial velocity. If the fall edge is too long, it may result in the droplet coming back into contact with the injector and coalesce with the next droplet of fuel and forming a barrier of liquid fuel that remains attached to the end of the injector and prevents new droplets from being created. Voltage is the most impactful function generator parameter regarding the creation of droplets. If the voltage is set too low, no droplets are created. If the voltage is set too high, instead of single isolated droplets multiple droplets or a spray is created. The waveform parameter of delay has no impact on the generation of droplets and is used only to align the droplet creation with the cameras used in image gathering.

The creation of droplets was subject to some day-to-day operational difficulties. These difficulties could be addressed by changes made to the function generator parameters as well as ensuring that there was no air or other gasses due to evaporation present in the system. If no droplets were created, either the voltage needed to be increased or there was air in the fuel line. If more than one droplet was produced, then the voltage needed to be lowered, the pulse width needed to be decreased, or the rise edge needed to be increased. If spraying was occurring, the voltage or pulse width needed to be decreased or the rise edge needed to be increased. If droplets were created for a brief period and then stopped, either the voltage or pulse width needed to be decreased, or the rise edge needed to be increased, or there was air in the fuel line. These minor issues were troubleshot as they occurred.

The droplets were ignited after leaving the injector by passing through a heating coil made of a nickel chromium (nichrome) alloy. Nickel chromium is a material commonly used in heating elements which is why it was selected for use in this system. The power supplied to the heating coil was controlled by a Variac Variable Transformer. The heating coil was positioned such that the center of the injector was aligned with the center of the coil. The heating coil was placed just prior to the inlet of the channel and was preceded by an aluminum honeycomb structure to promote laminar airflow at the inlet.

The converging channel was designed so that the decrease in cross-sectional area along the axial direction would promote acceleration of the air within the channel at a rate matching gravitational acceleration, 9.81 m/s^2 for a given initial velocity of 1 m/s. The curved pieces that compose the converging walls were originally designed and fabricated by DeMaio for his thesis research [23]. These pieces are machined from aluminum. The width of the channel remains constant at 1 inch (2.54 cm) for the entire axial length of 150 cm. The initial length of the inlet rectangular cross-section is 4 inches (10.16 cm) and decreases to a final length of 2.76 cm. The flat sides of the channel, the planar pieces, are made by panes of either glass or acrylic. The glass panes are located at the top of channel to address a previous problem of acrylic melting due to the proximity of the heating coil [23]. The acrylic panes are sealed to the metal pieces by bolts.

The overall structure of the experimental setup supports the channel as well as the heating coil and injector, as seen in Fig. [2.3]. The structure is made of extruded aluminum and has four vertical posts with connecting bars that can be affixed to the posts at various heights. The modular design of the structure with the aluminum bars allows for

simple modifications and additions for optical analyses. Two steel plates hold the converging channel in place: one at the top and the other at the bottom. The upper plate has an opening for the inlet of the channel and holds the heating coil. The injector is held above the upper plate by bolts fixed into the plate. These bolts allow for the injector to be moved up or down relative to the converging channel. The lower plate has a cylindrical metal container attached to its base which is connected to the pump via a hose and acts as the outlet of the channel. The container has another opening which is sealed from below which would allow for access to the end of the channel to clean the channel walls or collect samples. The plates are fixed to the supporting bars with standard metal D-clamps. A separate, smaller structure of similar design with aluminum bars and posts can be bolted to the tower frame and utilized for supporting the cameras used in the optical analyses.

The pump is attached to the bottom of the channel using a flexible aluminum hose. The pump utilized is an Intex Quick-Fill™ AC Electric Air Pump. This pump is appropriate for this application because it does not allow backflow and is designed to experience resistance to flow due to the original purpose of inflating or deflating air mattresses. The maximum air flow produced by the pump is 650 L/min.

To examine the droplets, two different cameras were utilized in this study. The first is a high-speed camera, the Photron Fastcam SA-Z camera, and was used to take images of the droplets with background light. Using a mirror and point source of light, a beam of collimated light was created behind the channel in front of the camera in order to see the shadow of the droplet. To take images of the flames, an Andor iStar ICMOS camera was used. The flame emissions were observed through a CH chemiluminescence

(CH*) filter. The ICMOS camera was triggered by a pulse waveform from the second output channel of the function generator with a delay to allow the droplet to fall to the section of channel under examination. The second output channel of the function generator was set with the same frequency and waveform as the first channel which controlled the piezoelectric actuator to ensure synchronization between the signals. This allowed the camera to capture images when the flames passed by.

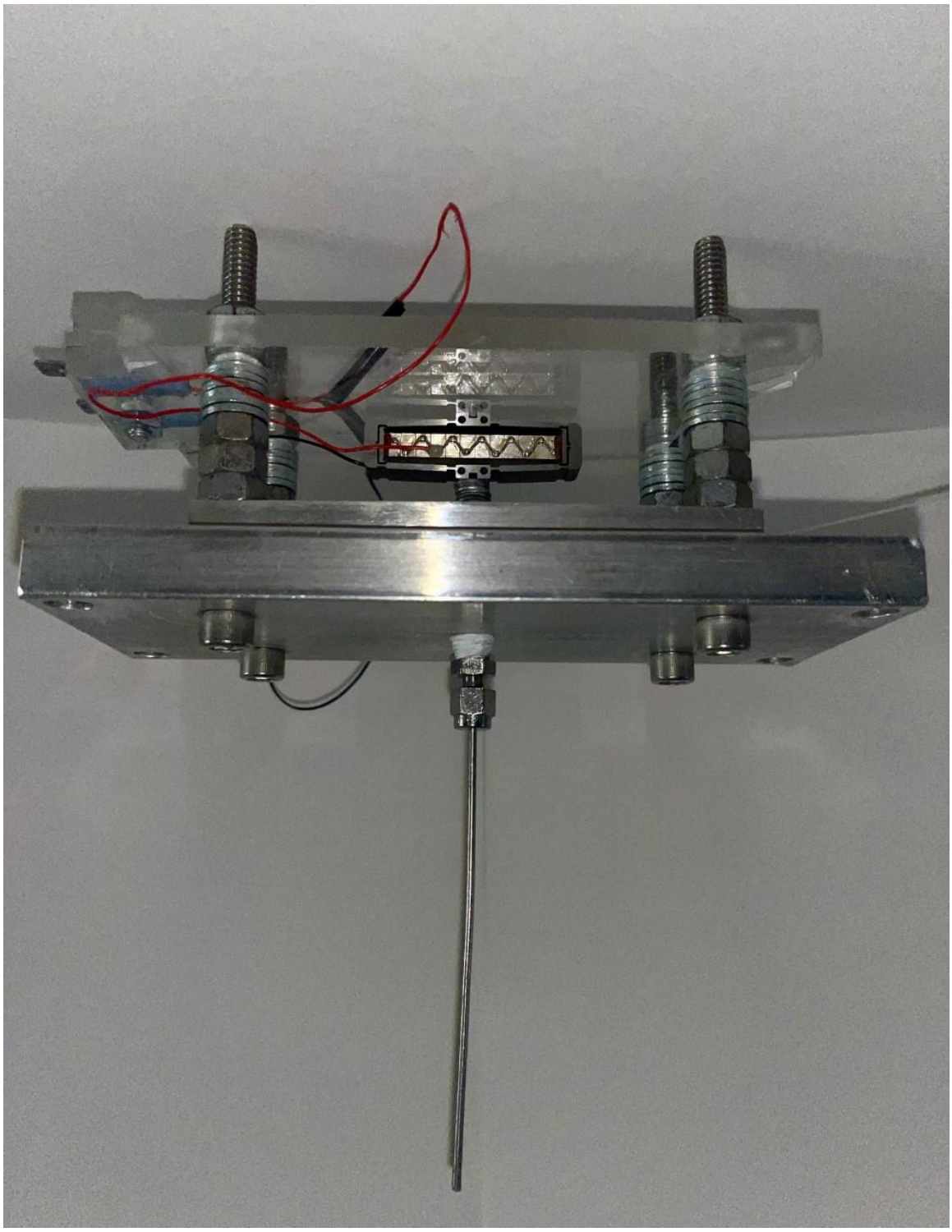

Figure 2.1 Droplet Generator and Injector

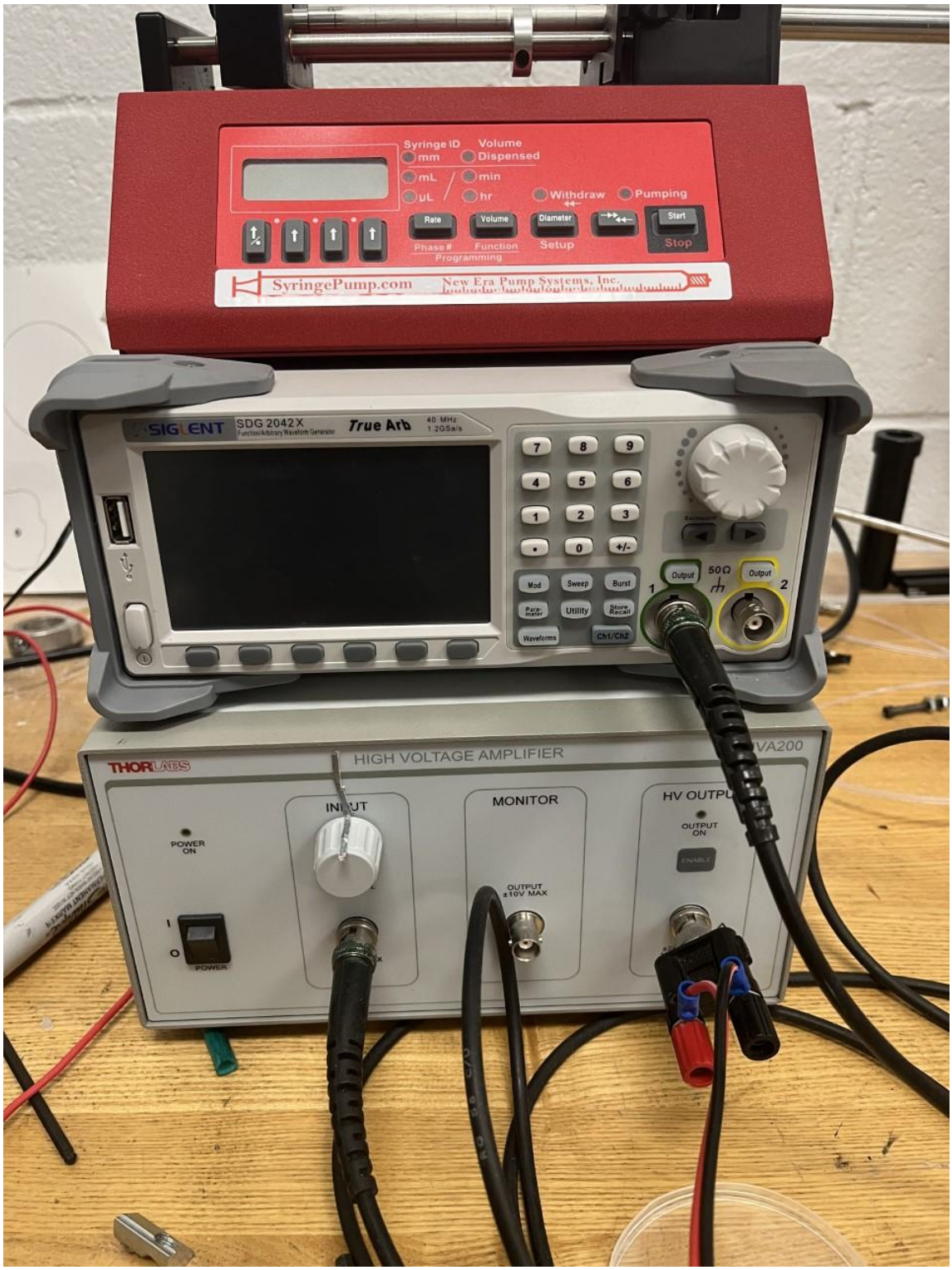

Figure 2.2 Syringe Pump, Function Generator, and Voltage Amplifier

Figure 2.3 Overall Experimental Setup

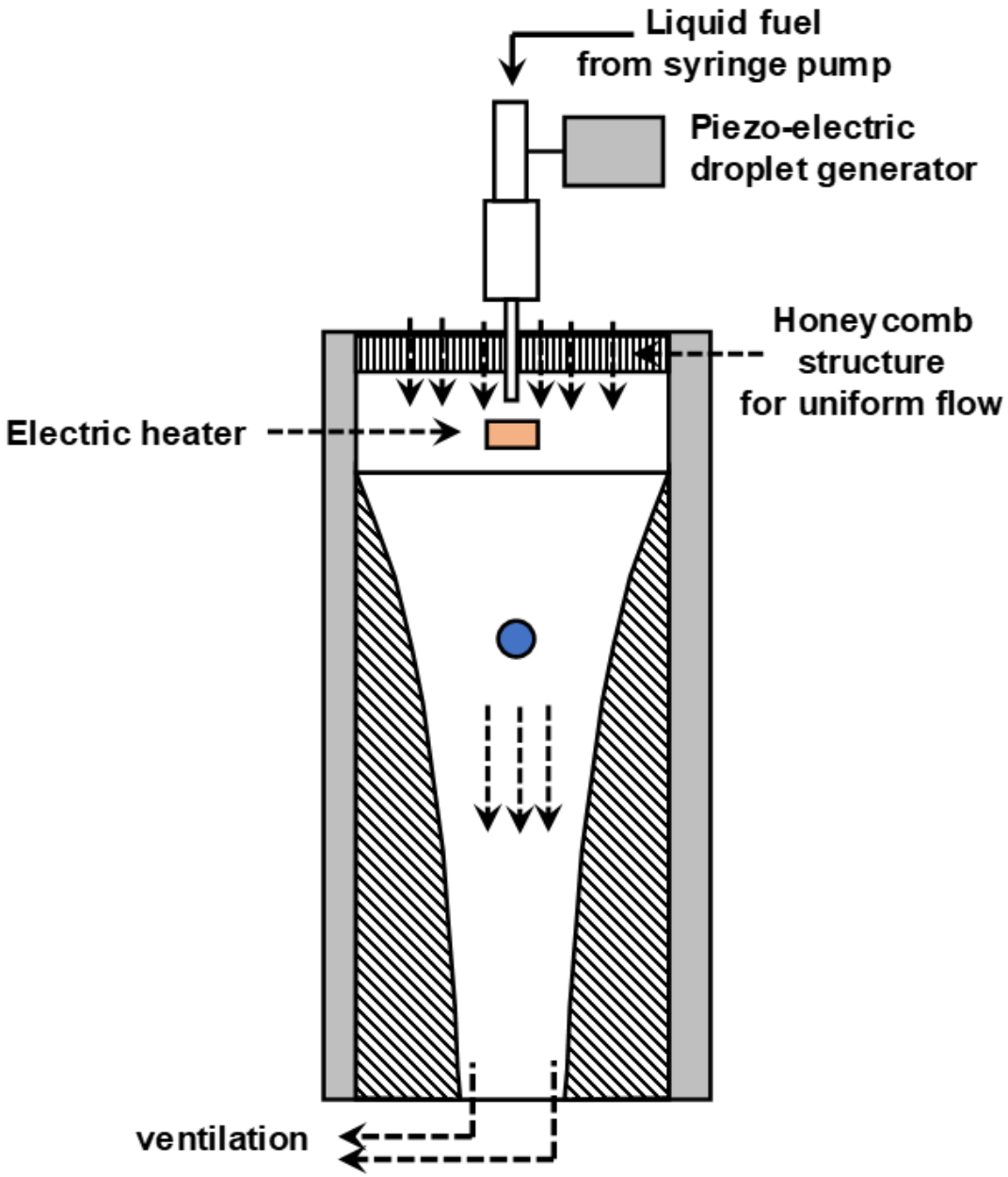

Figure 2.4 A Schematic of the Experimental Setup

CHAPTER 3
RESULTS AND DISCUSSION

The droplet generator and injector were specifically designed for this experiment, so the consistency in droplet size was measured to ensure precision. This was done by taking high-speed images of the droplets and using inherent image processing functions in MATLAB to measure the droplet diameter in pixels, which could then be converted to millimeters. The results from this experiment can be found in Table 3.1. Two different trials were conducted with varying frequencies and flowrates, holding droplet diameter constant according to equation 2.5. For both trials, the standard deviation of droplet size was extremely small, less than two thousandths. Additionally, the average diameter differed by less than two hundredths of a millimeter. Therefore, it can be concluded that the size differences between droplets are negligible, regardless of frequency and flowrate.

To verify spherical symmetry of the flame, the flowrate of air was calculated to match the experimentally determined initial velocity at the inlet of the tower. The velocity of non-ignited n-Heptane droplets was measured at different heights using high-speed imaging. From these points, the initial velocity of the droplets was calculated. The velocity determined for the droplets was compared to theoretical calculations based on an inviscid assumption, making use of one of the kinematic equations,

$$v^2 = v_0^2 + 2a\Delta x \tag{3.1}$$

for the air flow as seen in Fig. 3.1. The experimentally determined velocity was also compared to the air flow velocity using the curvature of the channel walls as a means of determining the acceleration experienced by the flow. The difference between the simplified inviscid assumption and the model based on the curvature can be seen in Fig. 3.2. The channel curvature velocity calculation was used to determine the air flow rate which would align with the desired initial velocity of 1 m/s, which had been validated by the experimental data.

At the calculated flowrate, experimental images of flames were obtained at various positions along the droplet stream trajectory. Both visual inspection and analysis performed through processing the images taken of the flames verified that spherically symmetric flame structure existed over the course of the droplet burning. The effects of varying air flowrates on flame geometry are shown in Fig. 3.3; the images were obtained with flowrates greater than, equal to, and less than the calculated flowrate.

The first fuel used in this study was n-Heptane. The initial droplet diameter produced for n-Heptane was 0.580 mm, which was experimentally determined by processing the images of unlit droplets obtained with the high-speed camera. Figure 3.4 displays the normalized droplet diameter squared as a function of the normalized time for various locations along the axial length of the channel. The droplet diameter was determined using image with background light with the high-speed camera and image processing performed in MATLAB. In MATLAB, the image was converted to a binary image, then an ellipse was fitted to the area of the droplet. The minor axis of the ellipse fitted to the droplet was used to approximate the diameter. Using the minor axis

eliminated any possible error due to blurring of the image, as the droplet was only moving in the vertical direction. A linear trend consistent with the d^2-law of droplet combustion was observed. However, the linearity is stronger in the upper section of the channel. Figures 3.5 and 3.6 include numerical simulation data for normalized droplet diameter squared and flame diameter compared to the experimental data. The linear trend of the droplet diameter experimental data has a more negative slope than the simulation data, indicating a greater burning rate. This could be due in part to the one-dimensional nature of the simulation and its lack of consideration for convective effects. Other possible reasons for the difference could be due to the dissolved gasses in the fuel or hotter than ambient gas flow due to the ignition source. For the flame diameters, a similar trend is observed between the experimental data and the numerical simulation results, though the simulation overestimates the experimental data. The diameter of the flame was measured using the ICMOS camera through a CH chemiluminescence (CH*) lens filter and image processing performed in MATLAB. The diameter of the flame was approximated by the average of the major and minor axes of an ellipse fitted to the image. Using an average of the major and minor axes was appropriate for the flame imaging because it was assumed to be spherical and the exposure time was directly controlled, unlike the droplet imaging. Again, the disparity between the measurements and numerical simulation can be attributed to the aforementioned reasons.

To investigate potential differences between the numerical simulation and experimental results, particularly regarding the increased burning rate, the flow characteristics inside the channel were examined. The primary purpose of examining the flow characteristics was to verify if the flow was laminar, as desired, or if there were

turbulent effects. To test this, an observable component needed to be added to the flow. The smoke produced from burning incense was utilized to examine the flow. Incense was utilized because the smoke particles are heavier than air, causing the smoke to fall downwards naturally. This allowed for the flow to be visualized. The incense was burned just prior to the inlet to the channel, in the same location that the droplet injector would occupy. Figure 3.7 demonstrates the observed transition from laminar flow to a region which experienced turbulent effects. This observed transition may contribute to the increased burning rate of the droplet since velocity fluctuations increase as result from turbulence and would encourage quicker burning.

Despite the differences between the n-Heptane experimental data and the numerical simulation, it may be concluded that the converging channel does have the ability to promote single isolated droplet combustion with spherical symmetry. To further verify the functionality of the channel, the experiment was repeated using ethanol rather than n-Heptane as the fuel. Due to differences in the fuel properties, the initial droplet diameter of ethanol was 0.681 mm. Figure 3.8 displays the normalized droplet diameter squared against normalized time to evaluate the agreement between the experimental data and the classical d^2-law of droplet combustion. The experimental data does not follow a linear trend as closely as the data for n-heptane demonstrated, as seen in the R^2 value for the linear trendline fit to the data for each fuel.

Figure 3.9 compares the normalized droplet diameter squared against normalized time for the experimental data as well as for a numerical simulation. The burning rate of ethanol outlined by the experimental data is approximately three times faster than that of the numerical simulation. This deviation from the numerical simulation was anticipated

due to the differences seen for n-Heptane as seen in Fig. 3.5 but the ethanol experimental data showed greater disagreement with the expected burning rate. Such a stark difference between the experimental data and the numerical simulation seems to agree with the conclusion that turbulent effects observed from the incense test are impacting the burning rate. The slope of the line for the normalized squared droplet diameter produced by the numerical simulation for ethanol experiences a sudden change at 1.7 s/mm^2 where the slope of the line levels out. This change in the slope indicates an extinction process, as the absence of a flame would result in evaporation being the cause of droplet diameter decrease which occurs more slowly than burning. The extinction process can also be observed on Fig. 3.10 which compares the experimental flame diameter with the numerical simulation. In Fig. 3.10 the sharp decrease in flame diameter seen by the simulation supports the extinction process conclusion. There is good agreement between the experimental data and the numerical simulation for the size of the flame diameter at the observed points.

Table 3.1 Comparison of Experimentally Determined Droplet Velocity to an Inviscid Model

Frequency	Average D	Standard Dev
5 Hz	0.611429801	0.001761405
10 Hz	0.592144821	0.00198778

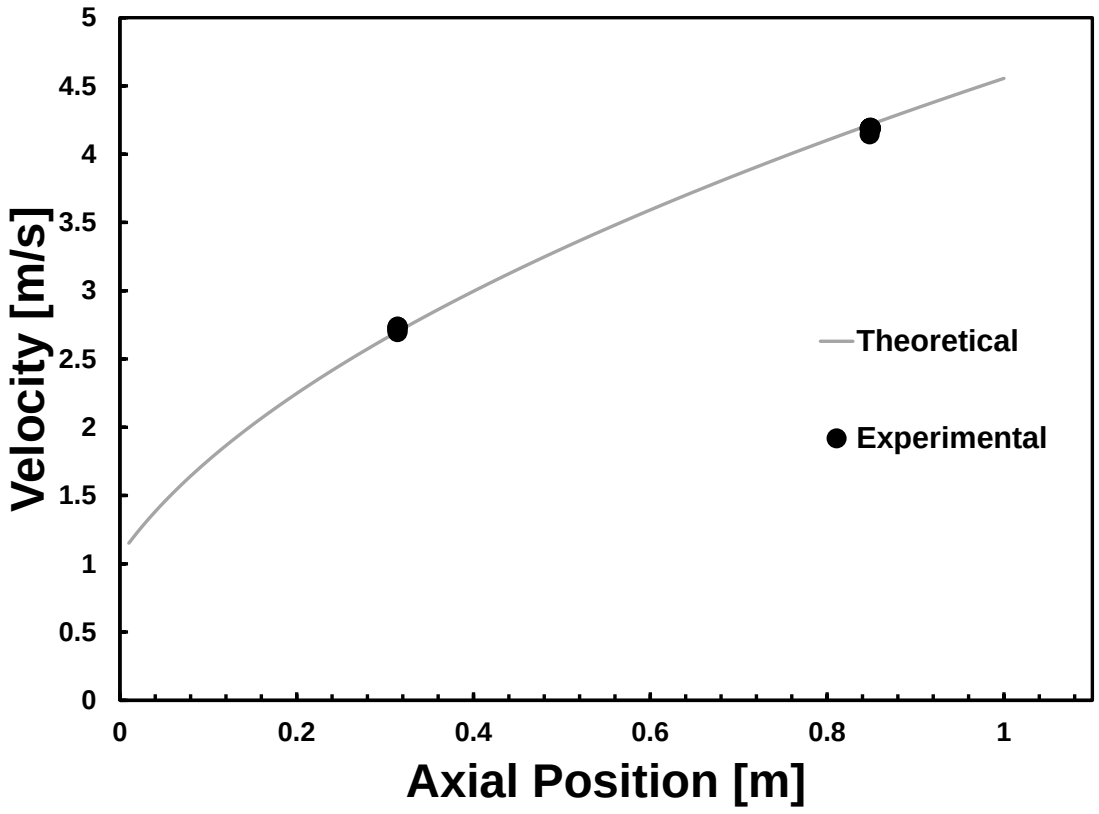

Figure 3.1 Comparison of Experimentally Determined Droplet Velocity to an Inviscid Model

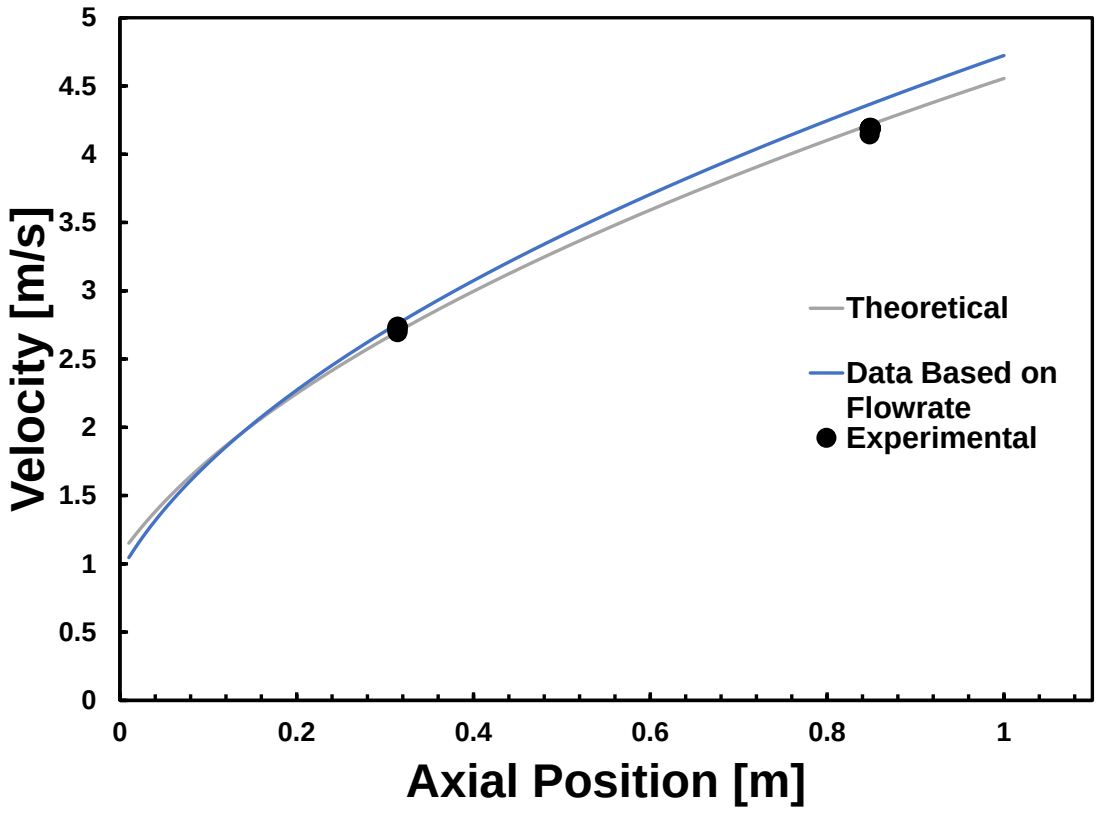

Figure 3.2 Comparison of Experimentally Determined Droplet Velocity to Velocity Derived from the Flowrate

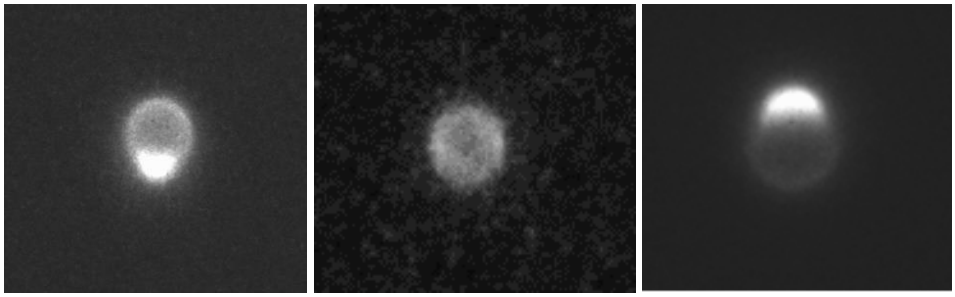

Figure 3.3 Illustration of the Effects of Flow Speed on Flame Symmetry

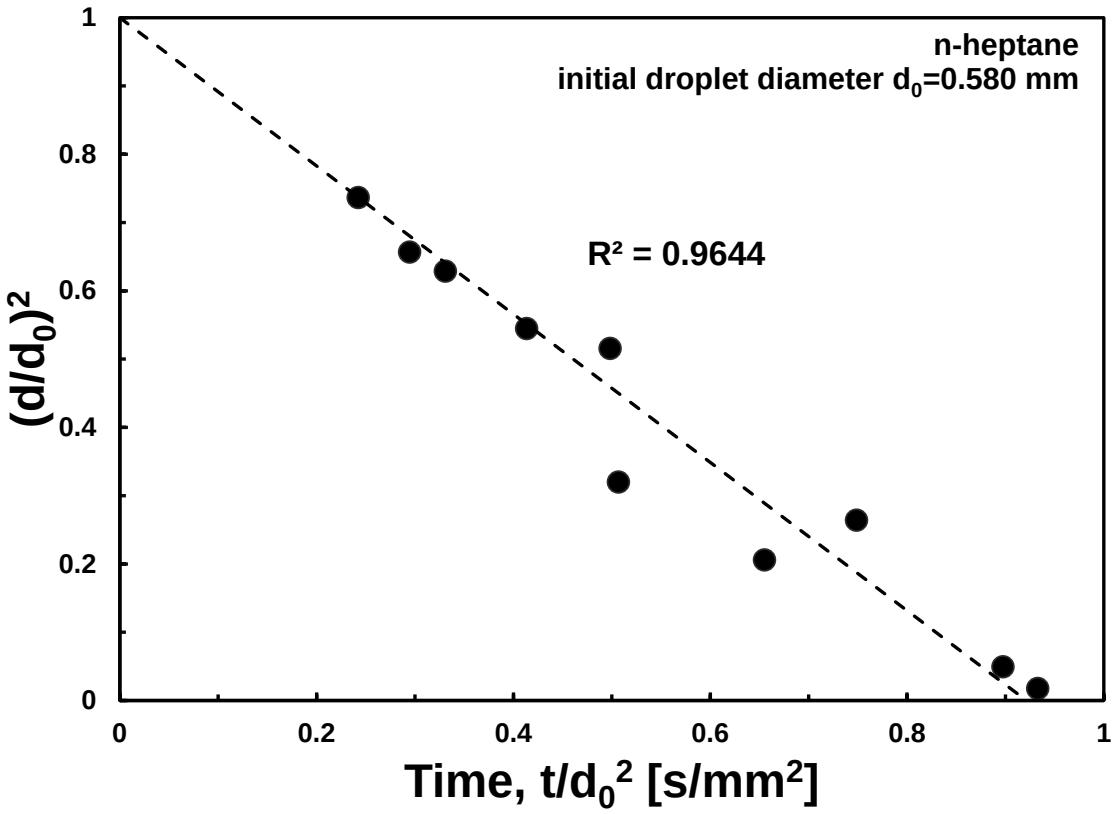

Figure 3.4 Experimentally Derived Data for Normalized Droplet Size Squared of n-Heptane Over Normalized Time

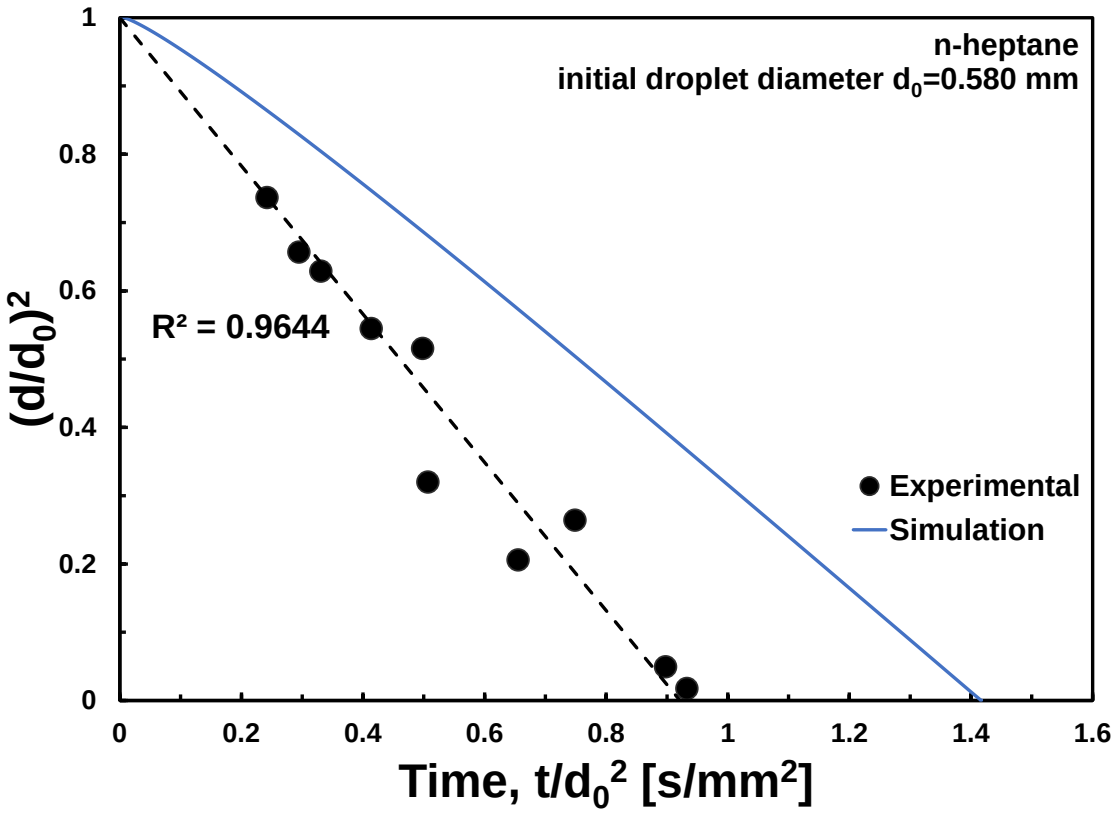

Figure 3.5 Experimental Data for Normalized Droplet Size Squared of n-Heptane Compared to Data from a One-Dimensional Simulation

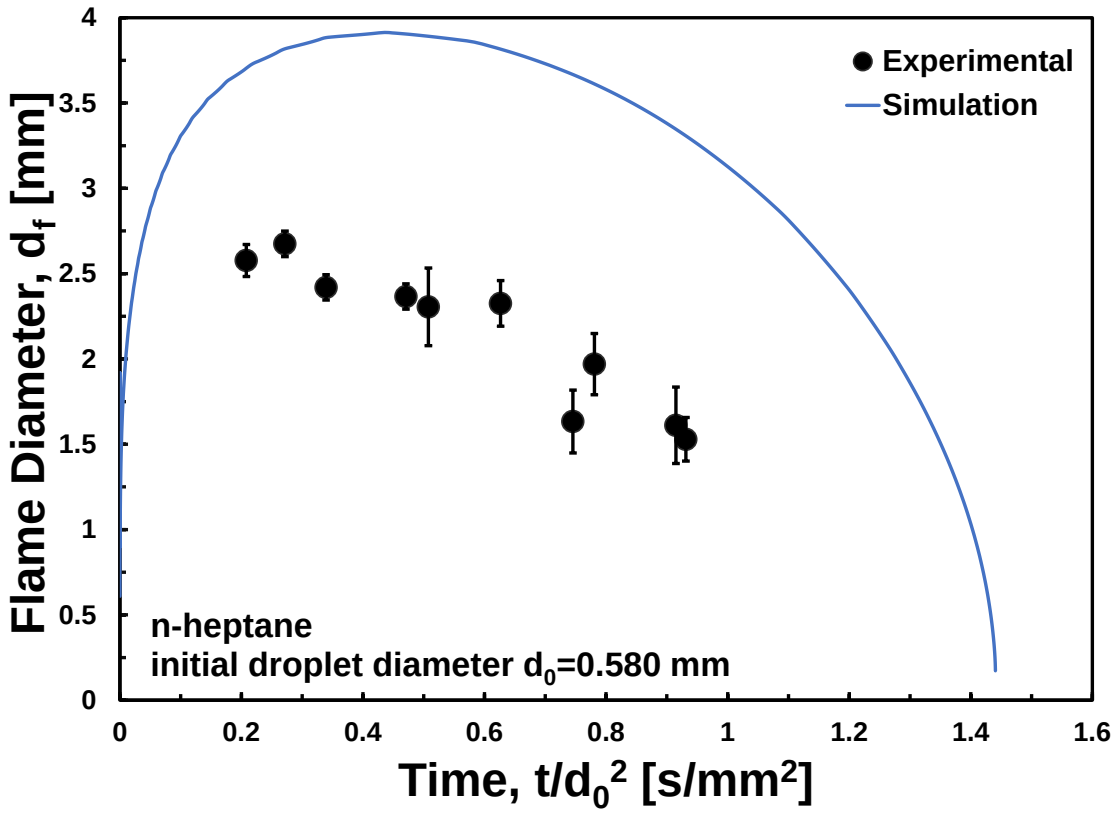

Figure 3.6 Experimental Data for Normalized Flame Size of n-Heptane Compared to Data from a One-Dimensional Simulation

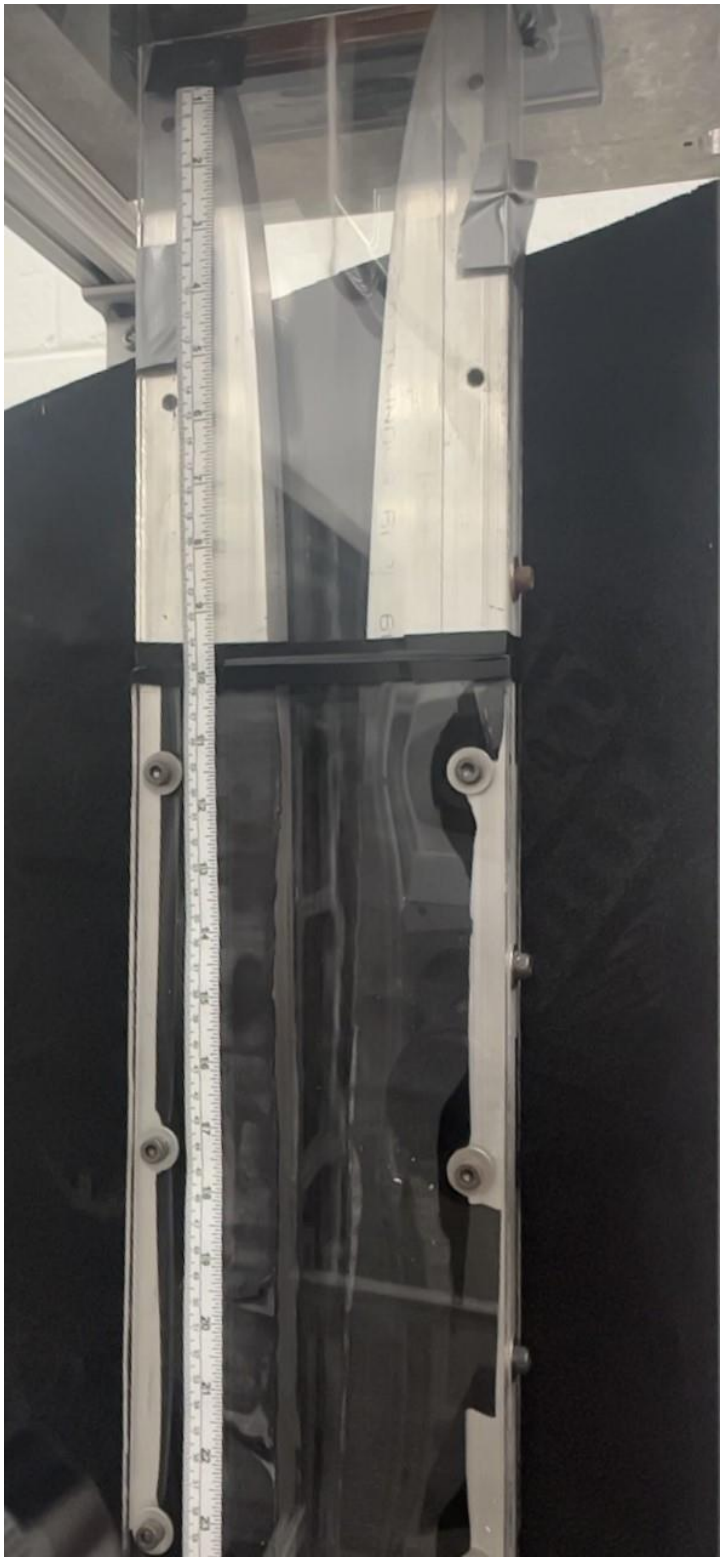

Figure 3.7 Incense Smoke Used for Flow Visualization

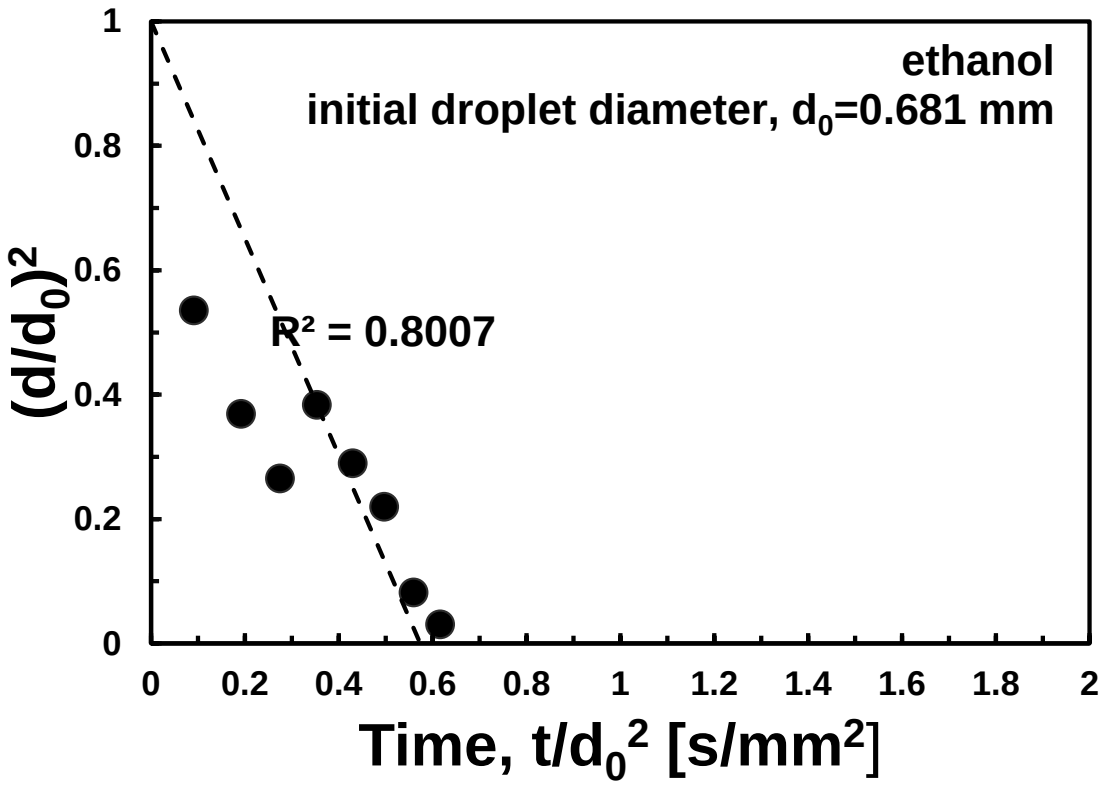

Figure 3.8 Experimental Data for Normalized Droplet Size of Ethanol

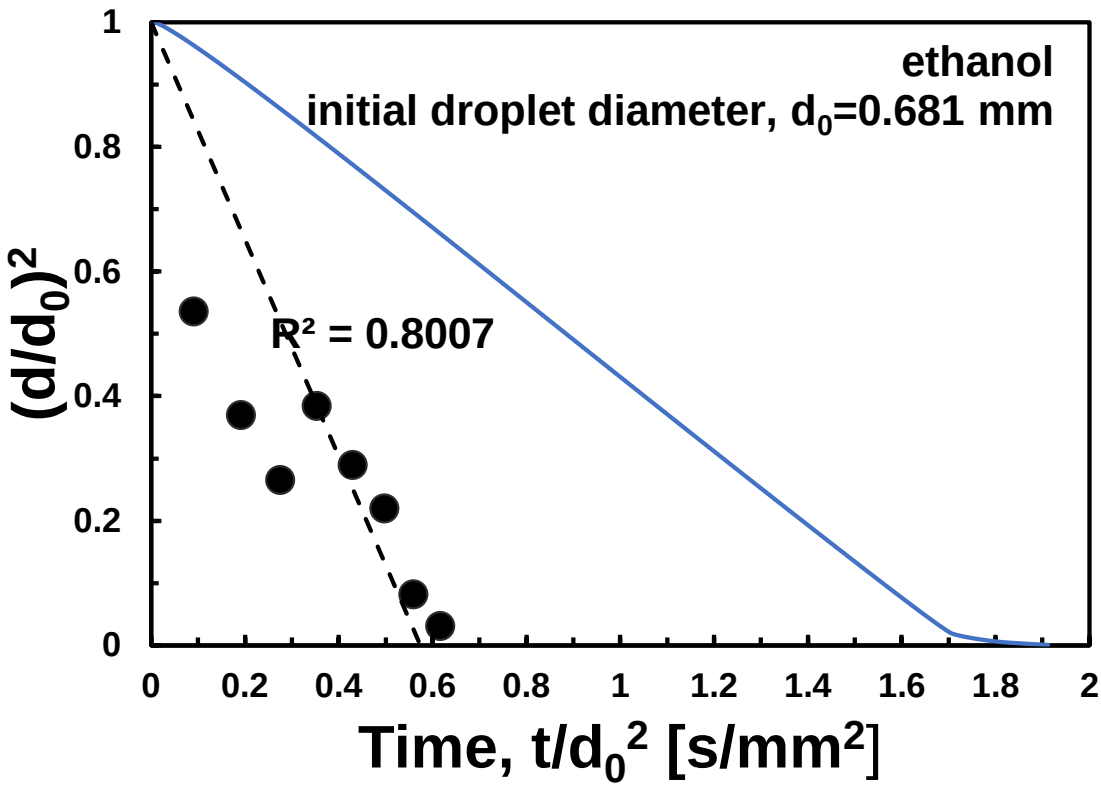

Figure 3.9 Experimental Data for Normalized Droplet Size of Ethanol Compared to Data from a One-Dimensional Simulation

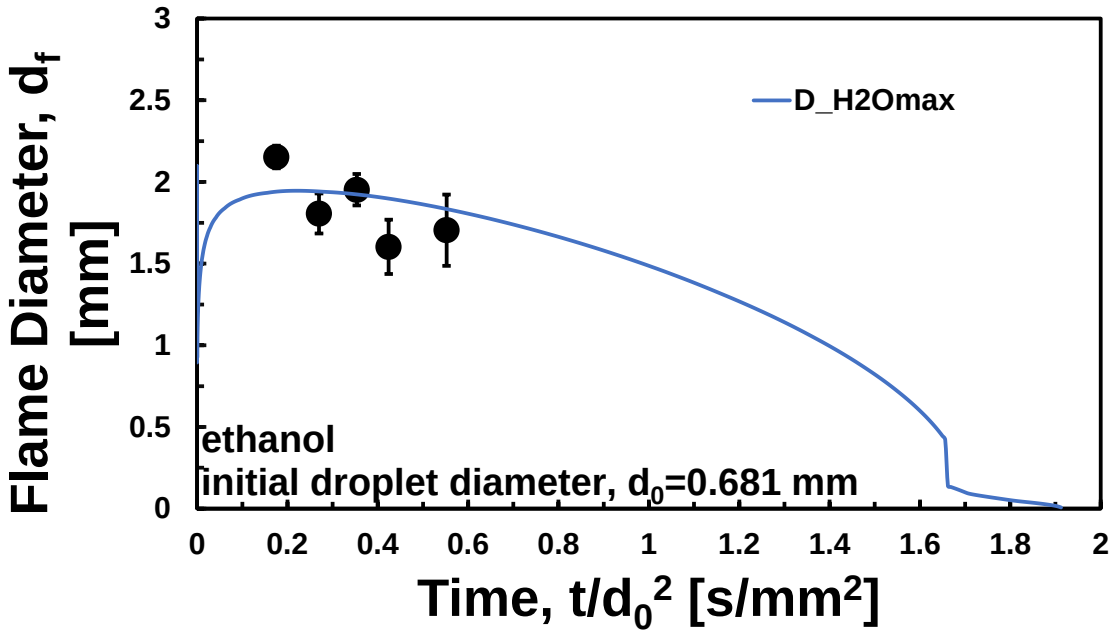

Figure 3.10 Experimental Data for Flame Size of Ethanol Compared to Data from a One-Dimensional Simulation Over Normalized Time

CHAPTER 4
CONCLUSION

This study verified the performance of a converging channel to promote spherically symmetric flames during isolated single droplet combustion. The channel was designed to minimize the effects of buoyancy by accelerating the burning droplet and surrounding flow to match gravitational acceleration. n-Heptane and ethanol were chosen as representative single component fuels. For each fuel, data was collected to evaluate the change in normalized diameter squared over normalized time. This relationship is comparable to both the classical d^2-law of droplet combustion and to data produced from a numerical simulation that was conducted in one dimension. There is clear deviation between the experimental results and the numerical simulation upon examination. An increase in the slope of the linear trendline applied to the experimental data in comparison to the slope of the numerical simulation results is most likely due to a faster than predicted burning rate.

In addition to examining the droplet diameter over time, the flame diameter over time was investigated. Flame spherical symmetry was evaluated using MATLAB image processing to analyze the CH* filtered imaging recorded with an ICMOS camera. There is a clear difference between the experimental results and the predicted flame diameter from the numerical simulation seen for n-Heptane. For ethanol, the trend of the flame

diameter experimental data reflects the results from the numerical simulation. The differences between the experimental flame diameter and the results of the numerical simulation for each fuel show a trend that is opposite to the differences between the experimental droplet diameter and the simulation results. For the flame diameter, the experimental data for ethanol is a better match to the simulation than for n-Heptane, but the opposite is true for the droplet diameter.

The disagreement between the experimental data and the numerical simulation may be due in part to the one-dimensional nature of the simulation. The simulation fails to consider convective effects, dissolved gases in the fuel, hotter than ambient gas flow due to the ignition source, and turbulent flow within the channel. The differences between the experimental results and the numerical simulation prompted an investigation into whether turbulence due to boundary layer growth on the planar surfaces of the channel could be the cause. A visual inspection of whether the air flow was laminar or turbulent was performed using smoke from incense to track the flow. This investigation concluded that the flow did not remain laminar as had previously been assumed. The fluctuations in velocity caused by turbulence could contribute to the increased burning rate of the droplets.

Despite the differences between the experimental data and the results of the numerical simulations, the converging channel was determined to succeed in its goal of creating a ground-based environment conducive for the study of spherically symmetric isolated single droplet combustion. The results support the need for further refinement in the experimental configuration to reduce the overall effects of the boundary layer growth in the channel. With refinements in methodology, future work may generate ground-

based data that includes sampling partially consumed droplets to investigate the effects of preferential vaporization of multicomponent fuel mixtures.

REFERENCES

[1] Godsave, G., *Combustion of droplets in a fuel spray.* Nature, 1949. **164**(4173): p. 708-709.

[2] Godsave, G. *Studies of the combustion of drops in a fuel spray—the burning of single drops of fuel*. in *Symposium (international) on combustion*. 1953. Elsevier.

[3] Goldsmith, M. and S. Penner, *On the burning of single drops of fuel in an oxidizing atmosphere.* Journal of Jet Propulsion, 1954. **24**(4): p. 245-251.

[4] Kumagai, S. and H. Isoda, *Combustion of Fuel Droplets.* Nature, 1950. **166**: p. 1111-1111.

[5] Kumagai, S. and H. Isoda. *Combustion of fuel droplets in a falling chamber*. in *Symposium (International) on Combustion*. 1957. Elsevier.

[6] Kumagai, S., T. Sakai, and S. Okajima. *Combustion of free fuel droplets in a freely falling chamber*. in *Symposium (International) on Combustion*. 1971. Elsevier.

[7] Okajima, S. and S. Kumagai. *Further investigations of combustion of free droplets in a freely falling chamber including moving droplets*. in *Symposium (International) on Combustion*. 1975. Elsevier.

[8] Knight, B. and F.A. Williams, *Observations on the burning of droplets in the absence of buoyancy.* Combustion and Flame, 1980. **38**: p. 111-119.

[9] Law, C.K. and G.M. Faeth, *Opportunities and challenges of combustion in microgravity.* Progress in Energy and Combustion Science, 1994. **20**(1): p. 65-113.

[10] Labus, T.L., *Natural frequency of liquids in annular cylinders under low gravitational conditions*. 1969: National Aeronautics and Space Administration.

[11] Shaw, B., et al., *Sooting and disruption in spherically symmetrical combustion of decane droplets in air.* Acta Astronautica, 1988. **17**(11-12): p. 1195-1202.

[12] Dietrich, D.L., et al. *Droplet combustion experiments in spacelab*. in *Symposium (International) on Combustion*. 1996. Elsevier.

[13] Dietrich, D.L., et al., *Droplet combustion experiments aboard the international space station.* Microgravity Science and Technology, 2014. **26**: p. 65-76.

[14] Farouk, T.I. and F.L. Dryer, *Isolated n-heptane droplet combustion in microgravity:"Cool Flames"–Two-stage combustion.* Combustion and Flame, 2014. **161**(2): p. 565-581.

[15] Kazakov, A., J. Conley, and F.L. Dryer, *Detailed modeling of an isolated, ethanol droplet combustion under microgravity conditions.* Combustion and Flame, 2003. **134**(4): p. 301-314.

[16] Marchese, A.J., F.L. Dryer, and V. Nayagam, *Numerical modeling of isolated n-alkane droplet flames: initial comparisons with ground and space-based microgravity experiments.* Combustion and flame, 1999. **116**(3): p. 432-459.

[17] Liu, Y.C., et al., *On the spherically symmetrical combustion of methyl decanoate droplets and comparisons with detailed numerical modeling.* Combustion and flame, 2013. **160**(3): p. 641-655.

[18] Farouk, T., et al., *Sub-millimeter sized methyl butanoate droplet combustion: Microgravity experiments and detailed numerical modeling.* Proceedings of the Combustion Institute, 2013. **34**(1): p. 1609-1616.

[19] Hara, H. and S. Kumagai. *The effect of initial diameter on free droplet combustion with spherical flame*. in *Symposium (International) on combustion*. 1994. Elsevier.

[20] Zhang, X., et al., *Some key technics of drop tower experiment device of National Microgravity Laboratory (China)(NMLC).* Science in China Ser. E Engineering & Materials Science, 2005. **48**: p. 305-316.

[21] Wang, D., J. Woo, and B. Shaw, *A drop-tube apparatus to promote spherically symmetric evaporation and combustion of unsupported droplets.* Review of scientific instruments, 1991. **62**(12): p. 3029-3036.

[22] Choi, M.Y., *Droplet combustion characteristics under microgravity and normal-gravity conditions*. 1992: Princeton University.

[23] DeMaio, N.A., *Development of a converging-channel drop tower for sphere symmetric isolated single droplet combustion*, in *Department of Mechanical Engineering*. 2021, University of South Carolina: Columbia, SC. p. 60.